XX Fluid Mechanics Conference KKMP2012,
Gliwice, 17-20 September 2012

ANALYSIS OF WIND PRESSURE DISTRIBUTION ON THE SURFACE OF 2:1 RECTANGULAR CYLINDER

Tomasz LIPECKI[1], Paulina JAMIŃSKA[2],
1Lublin University of Technology, Lublin, Poland;
2Lublin University of Technology, Lublin, Poland
E-mail: p.jaminska@pollub.pl

Abstract

The paper presents a study on the mean wind pressure coefficient distribution on surfaces of rectangular cylinders. The experiment was conducted in a closed-circuit boundary layer wind tunnel in the Wind Engineering Laboratory in Cracow, Poland. Several models were examined during the tests. This paper focuses on three models with the same side ratio of 2:1 (1:2), respectively of dimensions: 40 cm x 20 cm, 20 cm x 10 cm, 10 cm x 5 cm. The influence of aspect ratio for the same side ratio, wind structure parameters (profiles of mean wind speed and turbulence intensity and power spectral density functions) and the angle of wind attack on the wind pressure coefficient was examined.

Key words: wind tunnel, mean pressure coefficient, flow pattern, rectangular cylinder, wind structure, aspect ratio

INTRODUCTION

Wind action on tall buildings of square or rectangular cross-sections has been widely studied experimentally in wind or water tunnels, measured in full-scale and simulated numerically. In general, model investigations considered 2D or 3D models more often of square than of rectangular cross-sections. One of the main techniques used in measurements in wind tunnels is pressure measurement. Some papers considering the flow around rectangular models of side ratio of 1:2 (0.5) or 2:1 (2) are summarized below.

Analyses of various problems based on surface pressure measurements in case of 2D flow were presented by: Li and Melbourne (1999) (rectangles with side ratios of 0.5, 0.63, 0.8, 1, 2, 4, the influence of turbulence), Miyata and Miyazaki (1979) (rectangles with side ratios of 1, 0.5, 0.67, the influence of turbulence), Nakamura and Hirata (1989) (rectangles with side ratios of 0.2, 0.3, 0.4, 0.5, 0.6, 0.8, 1, vortex excitation).

Measurements focused on various aspects of wind action on 3D models were investigated by: Wacker (1994) (rectangles with side ratios of 3, 2, 1.5, 1, 0.67, 0.5, 0.33, and different heights), Liang et al. (2002) and Liang et al. (2004) (rectangles with side ratios of 1, 2, 3, 4 and different heights), Lin et al. (2005) (square and rectangles of side ratios 0.34, 0.5, 0.63, 1, 1.59, 2, 2.98, the influence of elevation, aspect ratio and side ratio), Tamura et al. (2008) (square and rectangles with side ratios of 0.34, 0.4, 0.5, 1 and different heights, angle of wind attack), Cheng and Tsai (2009) (square and rectangles with side ratios of 0.2, 0.25, 0.33, 0.5, 1, 2, 3, 4, 5 and aspect ratios of 3, 4, 5 ,6 and 7, different boundary layers), Zhang and Gu (2009) (rectangles with side ratios of 1, 0.67, 0.5, 0.33, 1.5, 2, and 3, two cases of boundary layer).

This study considers the differences in the wind action associated with the changes of the angle of wind attack, aspect ratio of the model with side ratio of 2 (0.5). Moreover the influence of the approaching flow characteristics was examined here.

RESEARCH DESCRIPTION

The experiment was conducted in a closed-circuit boundary layer wind tunnel in the Wind Engineering Laboratory in Cracow, Poland. Five models were examined during the tests. Dimensions of models are collected in Table 1, where *H*, *B*, *D* – are respectively: height of the model and length and width of the cross-section, so that *H*/*B* is defined as the aspect ratio, *B*/*D* is the side ratio. Models with the same side ratio – 1:2 (2:1) (R1, R3 and R5) are considered in this paper.

Each model was placed vertically on the rotational table in the centre of the measuring section as it is showed in Figure 1. The angle of wind attack was changed every 15° in the range 0°-90°. At 0° the longer side of the cross-section was placed perpendicularly to the mean wind speed direction.

Pressure points were installed on 16 levels. At each level 28, 28 and 20 pressure taps were located on circumferences of respective models R1, R3 and R5. The distributions of pressure points along the height of the model and around circumference as well as wind tunnel views of models R1 and R3 are presented in Figure 2. The data from pressure taps was archiving with 500 Hz frequency in the time range of 30 sec, which gave 6000 time steps.

Table 1. Model dimensions.

Model	*H*	*B*	*D*	*H*/*B*	*B*/*D*
	[cm]	[cm]	[cm]	[-]	[-]
R1	**100**	**40**	**20**	**2.5**	**2**
R2	100	40	10	2.5	4
R3	**100**	**20**	**10**	**5**	**2**
R4	100	20	5	5	4
R5	**100**	**10**	**5**	**10**	**2**

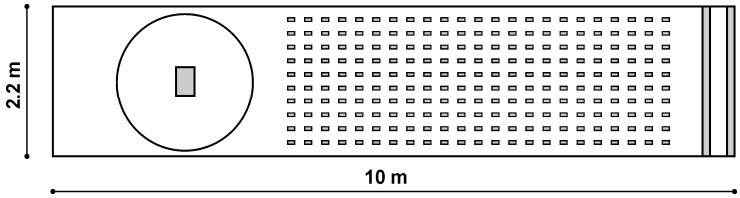

Figure 1. Wind tunnel set-up.

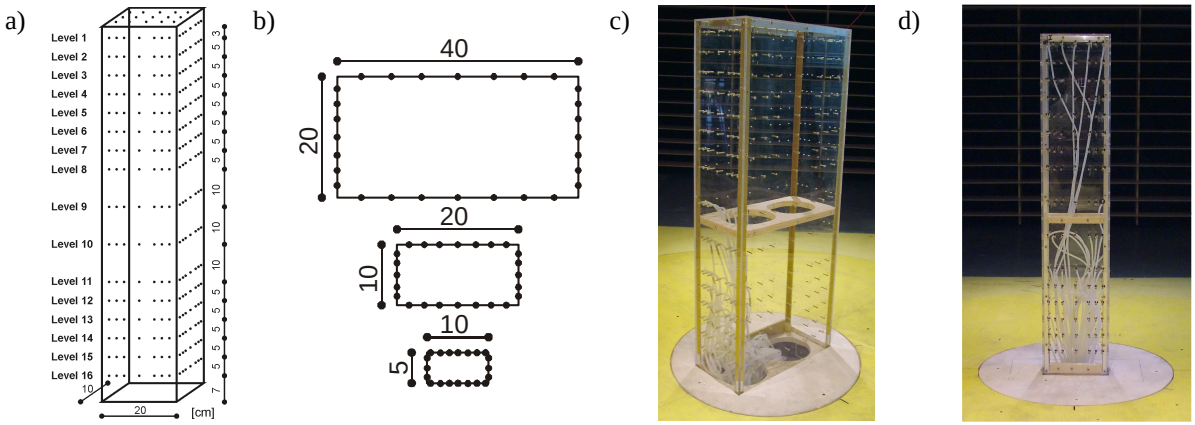

Figure 2. Experimental set-up: a) distribution of pressure points along the height, b) circumferential distribution of pressure points, c) models in the wind tunnel (R1, R3).

The flow in the wind tunnel was simulated by the use of wooden barriers, spires and blocks. All tests were performed in six different cases of wind structures characterized by mean wind speed profile, turbulence intensity profile and power spectral density functions. Detailed information on wind structure is presented in papers by: Bęc et al. (2011a, 2011b) and Lipecki and Jamińska (2012).

The mean pressure coefficient has been calculated using the following equation:

$$C_p = \frac{p}{0.5 \cdot \rho \cdot v_0^2}, \tag{2}$$

where: p – mean dynamic pressure measured in the given location on the surface of the model, $0.5\rho v_0^2$ – reference mean dynamic pressure, ρ = 1.25 kg/m^3 – air density, v_0 – wind speed in undisturbed flow in reference point, at the front of the model, at the height z = 70 cm.

RESULTS

Values of mean wind pressure coefficient C_p are presented for case of the model R3 (20 cm x 10 cm). Model façades denotation and angle of rotation used in the presentation of results are explained in Figure 3. The longer wall is always perpendicular to the mean wind speed direction in the position 0°. The windward wall in that position is marked as A, side walls – B and D, the leeward wall – C. For angle of wind attack equal to 90° wall D is windward, A and C – side walls, B – leeward wall. In cases of the wind attack angles 0° or 90° only one of side walls (B for 0°, A for 90°) is presented because of almost symmetrical distributions of C_p. The same settings for limits of C_p value are kept in every figure (max – 1.6, min – -1.8) according to the enclosed legend. Surface changes in the value of C_p in relation to the angle of wind attack are presented in Figure 4 in case of profile 1. Differences in C_p according to the wind structure are compiled in Figure 5 in two cases of the angle of wind attack: 0° and 90°. Figure 6 shows C_p surface distributions for all three models (R1, R3, R5), for angles of wind attack equal respectively to 0° and 90° and in two cases of wind structure – profiles 1 and 6.

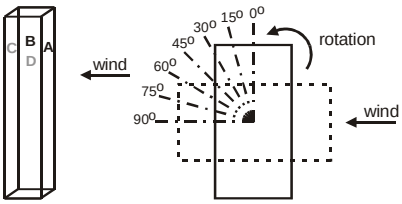

Figure 3. Wall and measurements denotations.

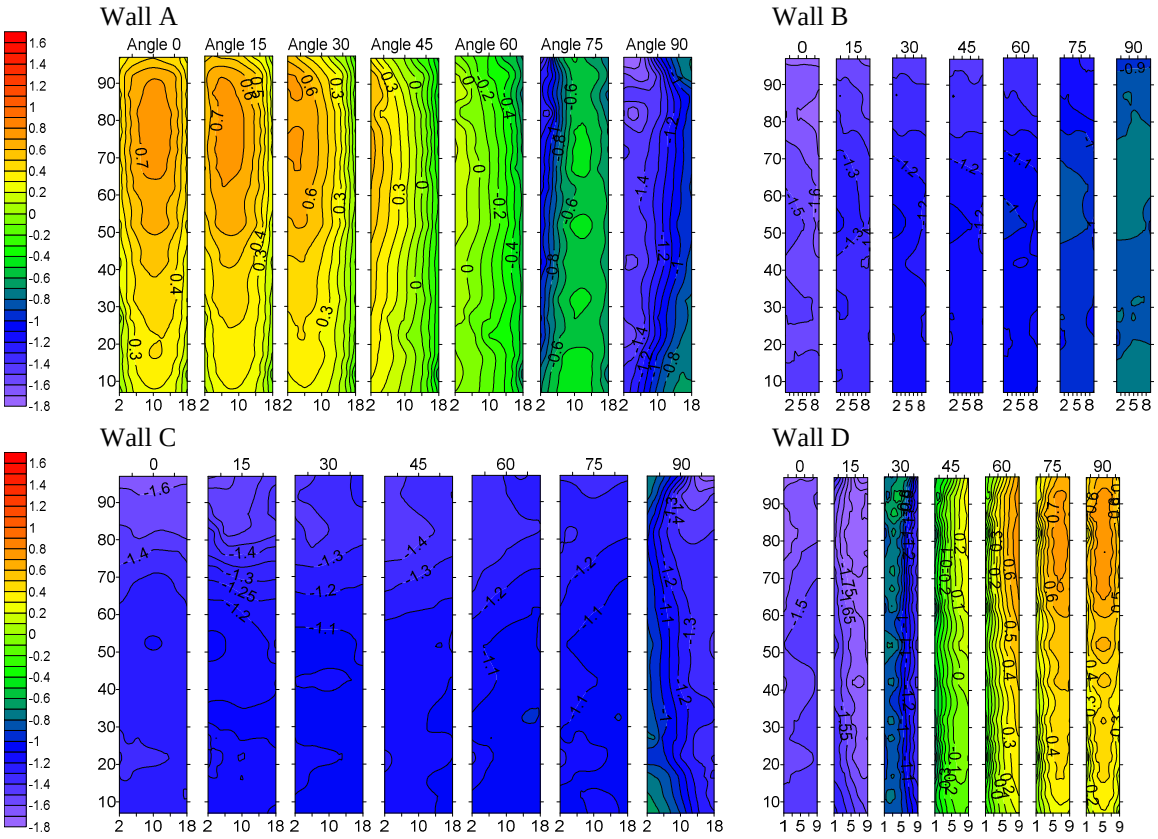

Figure 4. Pressure coefficient C_p, model R3, profile 1, in relation to the angle of wind attack.

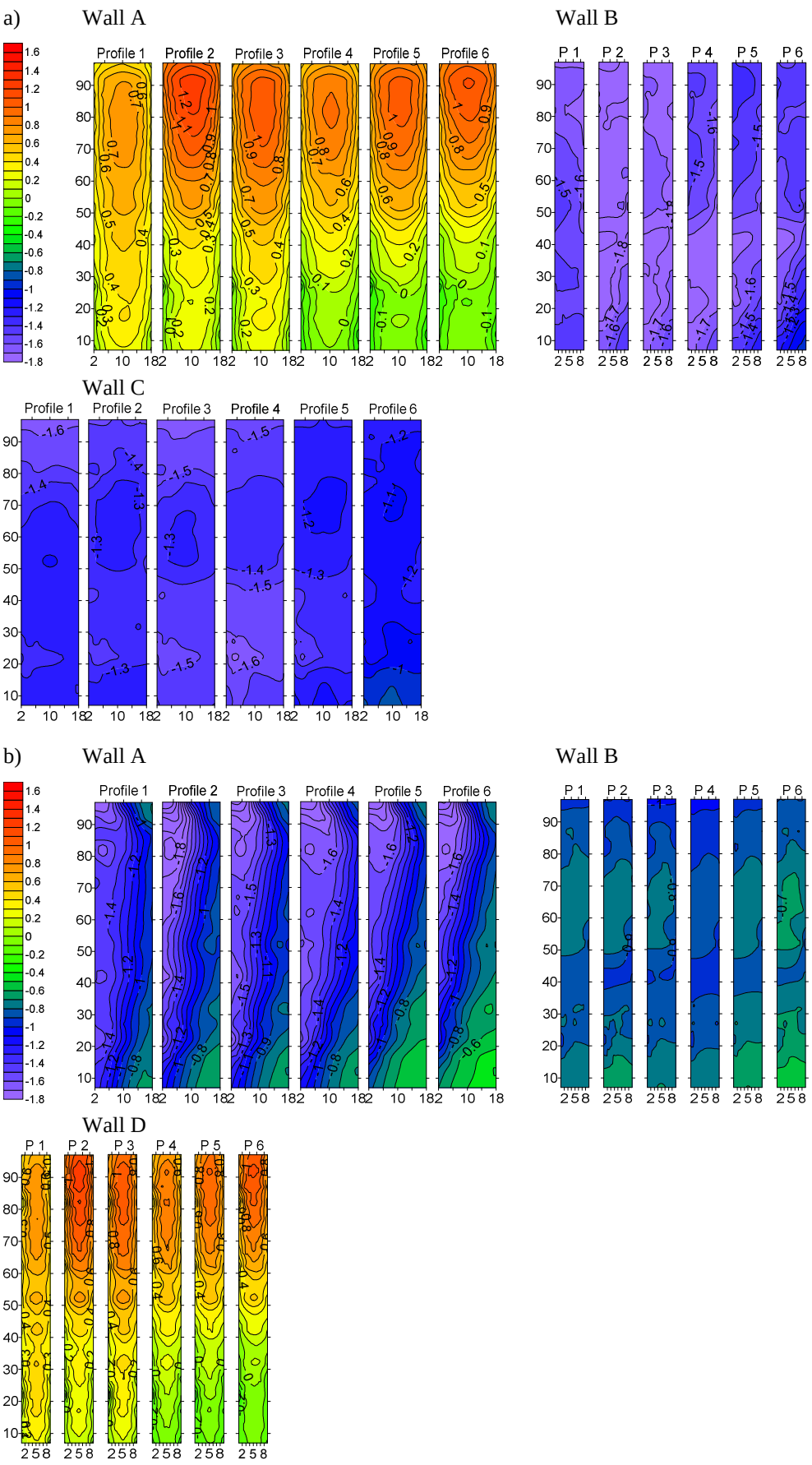

Figure 5. Pressure coefficient C_p, model R3, in relation to the wind structure, angle of wind attack equal to: a) 0°, b) 90°.

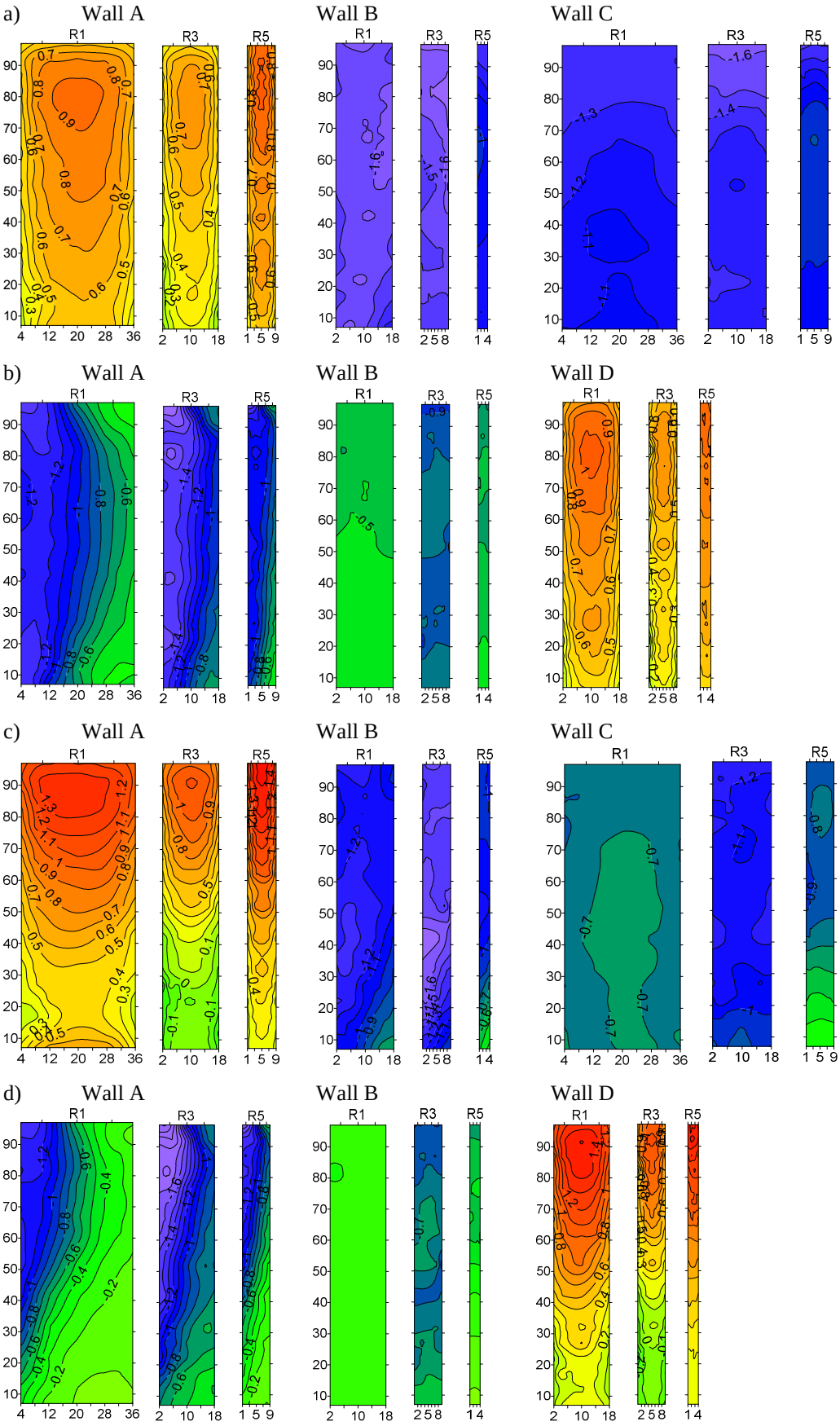

Figure 6. Pressure coefficient C_p, all models with side ratios of 2:1, a) 0°, profile 1, b) 90°, profile 1, c) 0°, profile 6, d) 90°, profile 6.

Circumferential distribution of the mean wind pressure coefficient C_p is presented in Figures 7, 8 and 9 respectively for angles of wind attack equal to 0º, 45º and 90º for five levels distributed along the height (Level 1 – 97 cm, level 4 – 82 cm, level 8 – 62 cm, level 12 – 27 cm, level 16 – 7cm) in dependence on the approaching flow characteristics. The legend with denotations of the cases of profiles is enclosed below.

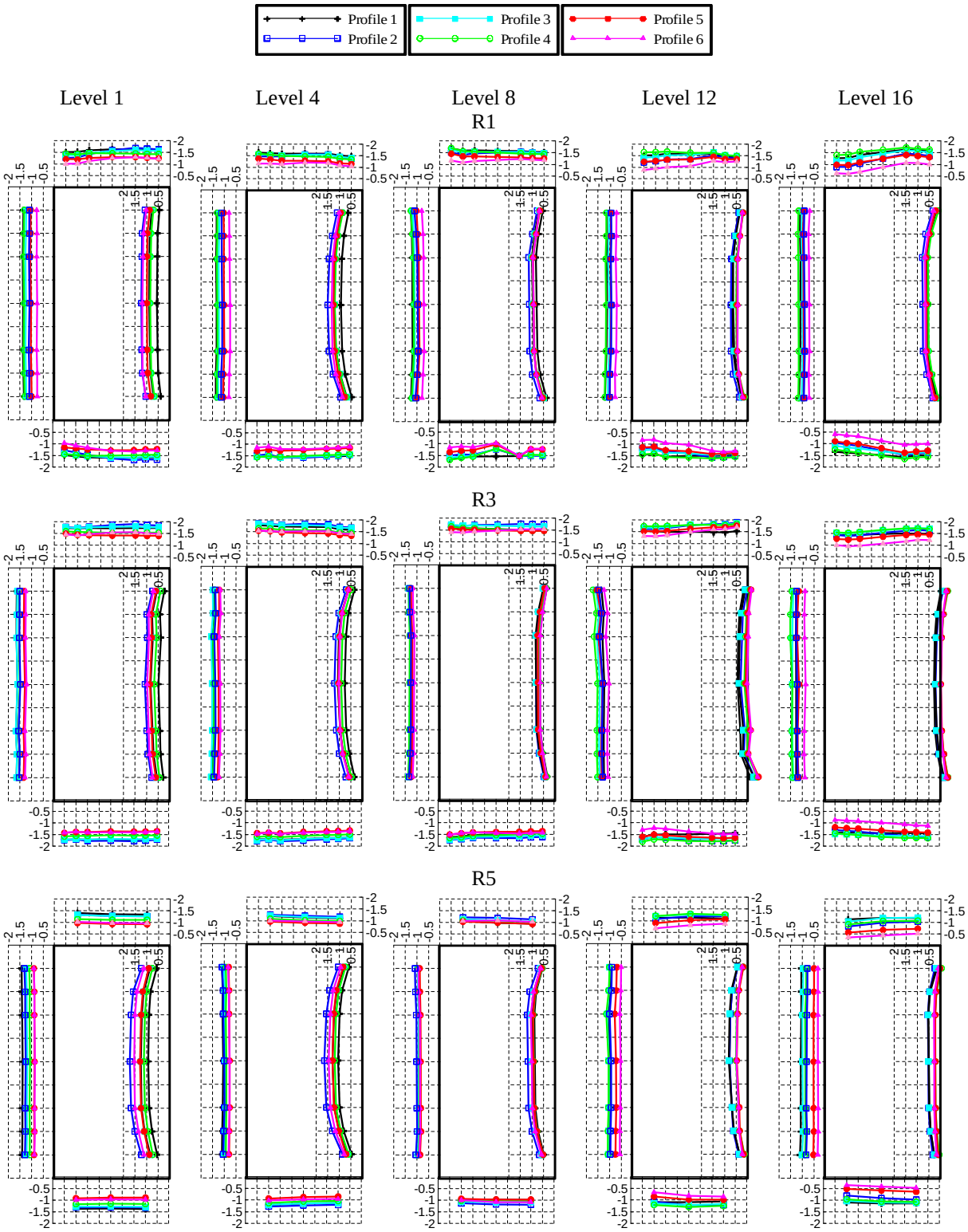

Figure 7. Circumferential distribution of C_p for all models R1, R3, R5, for the angle of wind attack 0°, in relation to the wind structure, on exemplary levels.

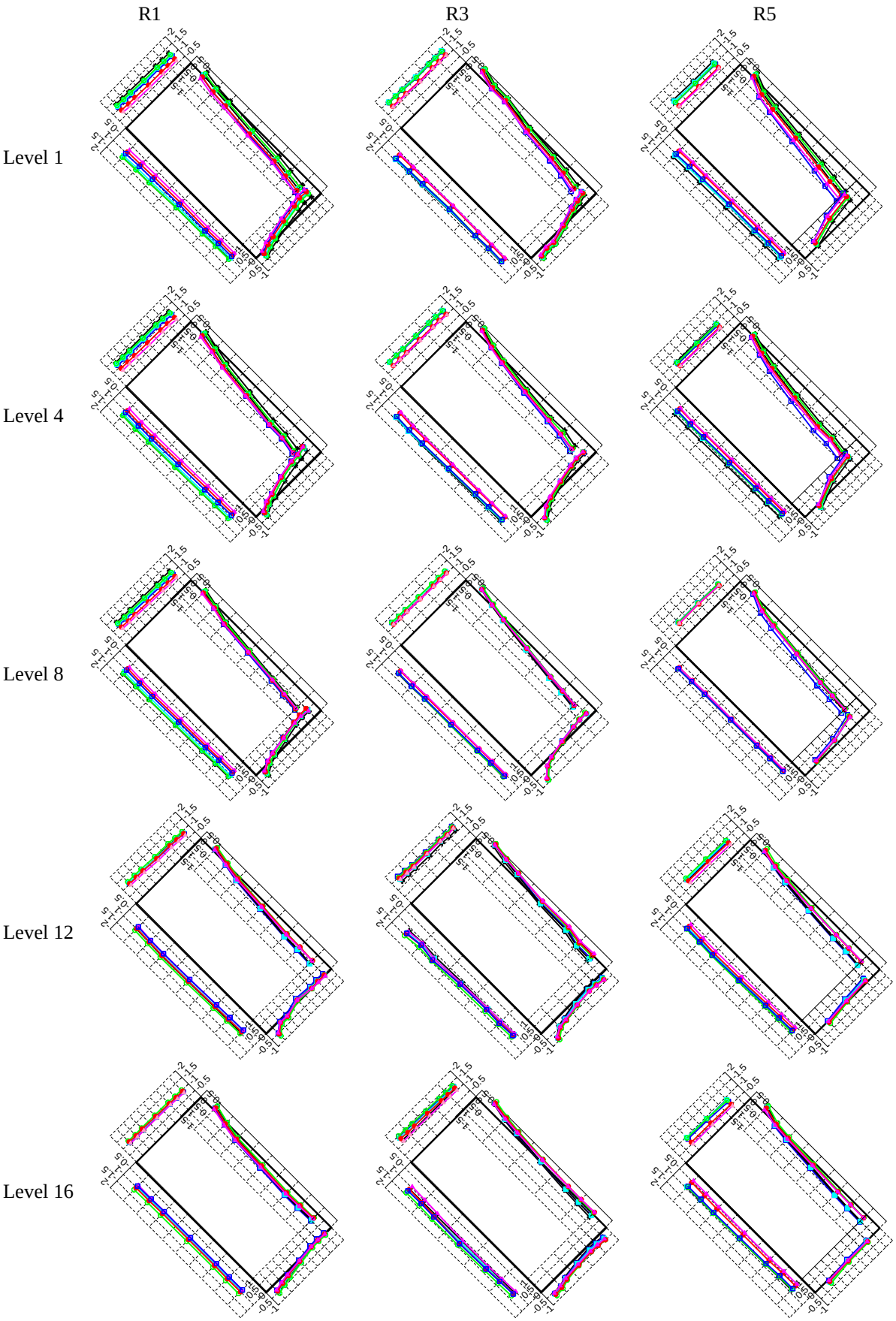

Figure 8. Circumferential distribution of C_p for all models R1, R3, R5, for the angle of wind attack 45°, in relation to the wind structure, on exemplary levels.

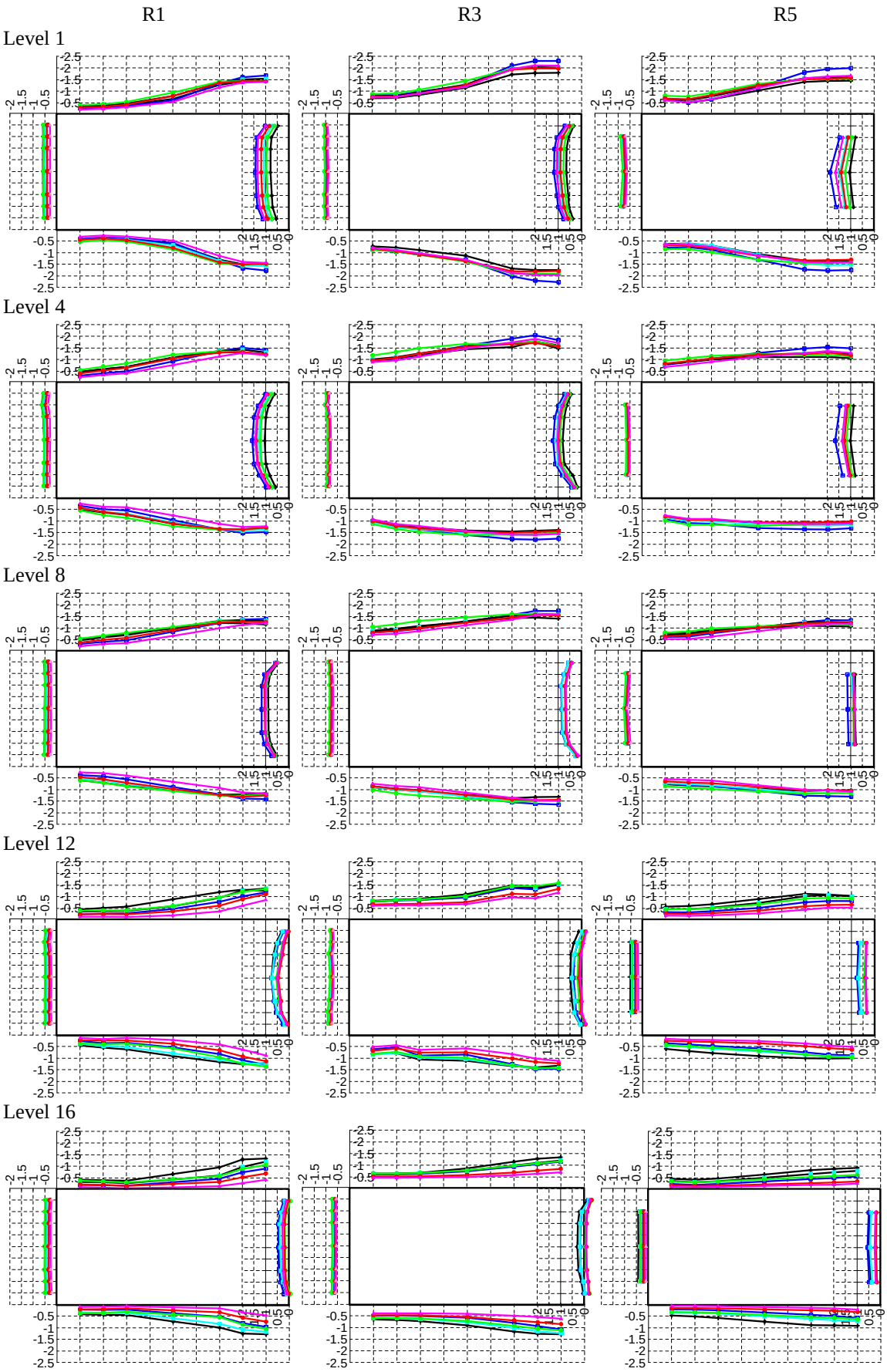

Figure 9. Circumferential distribution of C_p for all models R1, R3, R5, for the angle of wind attack 90°, in relation to the wind structure, on exemplary levels.

Vertical distributions in various locations around models circumferences were calculated in order to emphasize the differences in C_p values connected with the wind structure. Vertical distributions with locations of points are presented in Figures 10 and 11 for two cases of the angle of the approaching flow equal to 0° and 90°.

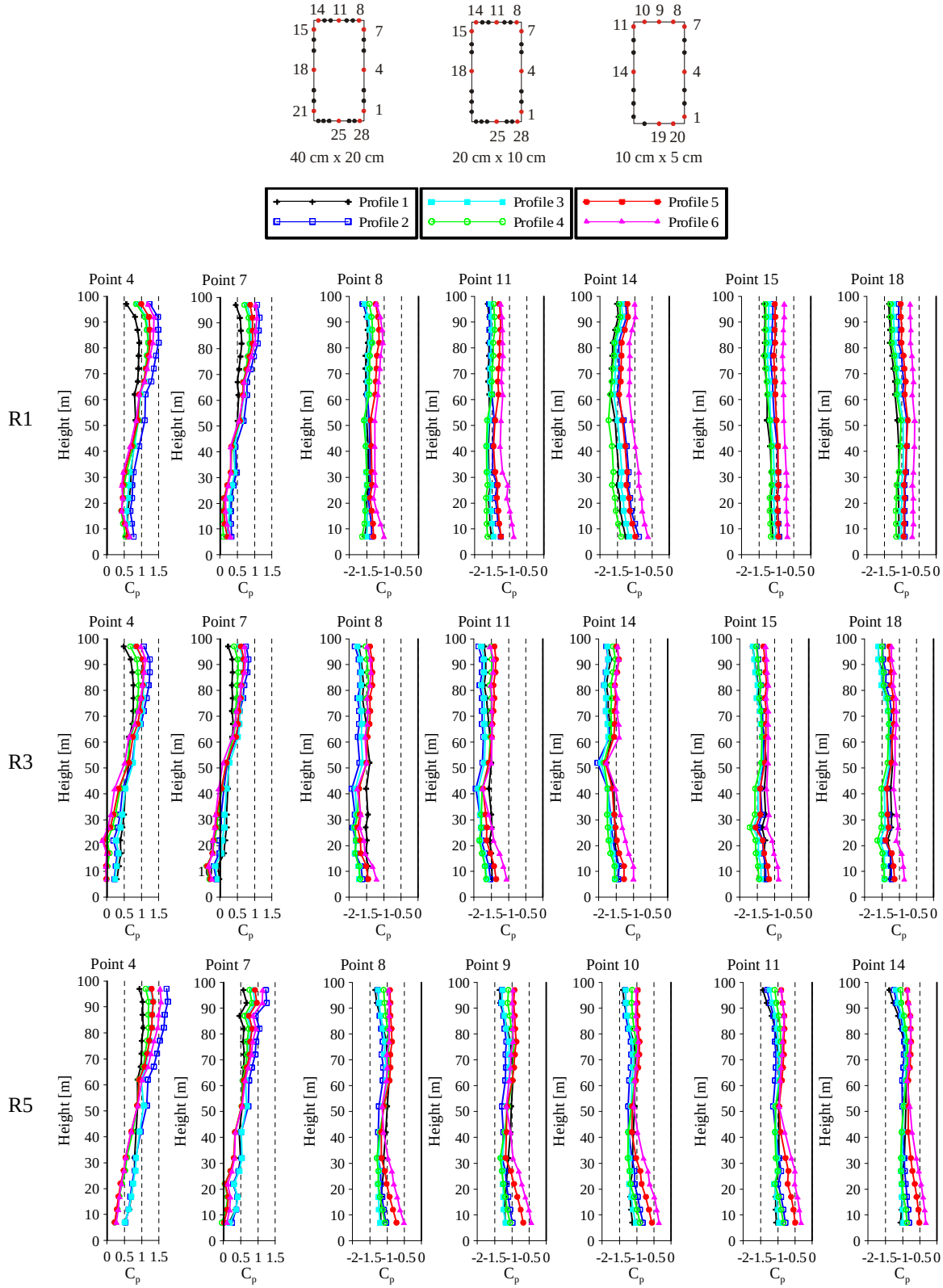

Figure 10. Vertical distribution of C_p for the angle of wind attack 0°, in points near edges and in the centre of each wall in relation to the wind structure.

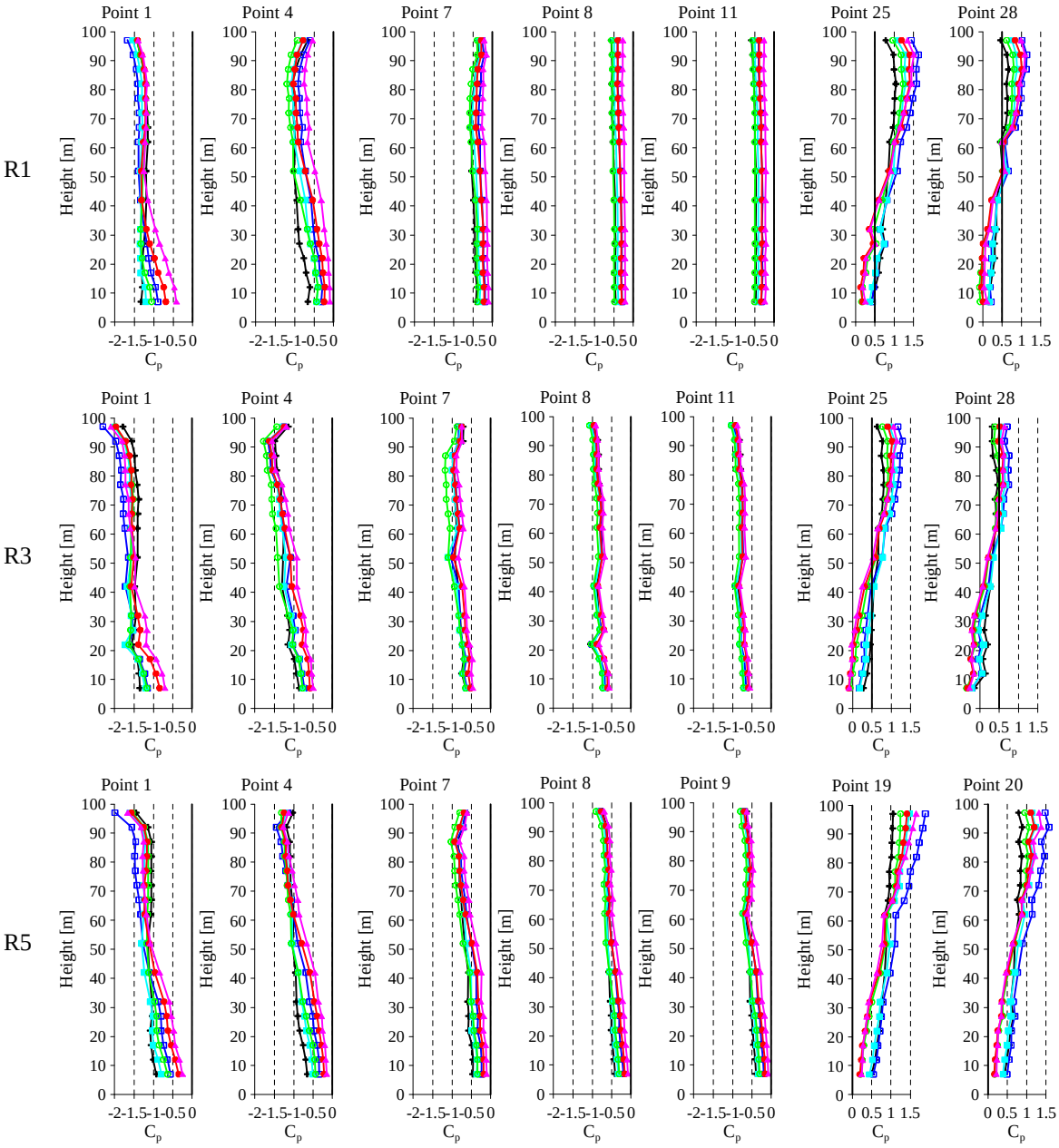

Figure 11. Vertical distribution of C_p for the angle of wind attack 90°, in points near edges and in the centre of each wall in relation to the wind structure.

All three sets of plots illustrate changes of pressure coefficient distribution along the height and around circumference of models with side ratio of 2:1.

For angles of wind attack equal to 0° and 90° pressure distributions are symmetrical, pressure occurs on the windward wall, and suction occurs on the side and the leeward walls. The highest values of pressure occur in the middle of the windward wall at a height of about 80-90% of the model independently of the wind structure. The decrease of pressure appears above this level due to the 3D character of the flow around the free-end of the model. On levels lying closer to the base of the model, roughness of the terrain increases, and thus the flow turbulence and friction in the boundary layer also increase causing a reduction in wind velocity and then surface pressure. Suction may occur on the windward wall near the edges at the lowest levels. Values of C_p on the windward wall also changes along the circumference and reduces close to the edges of the wall.

Vortex detachment appears at the edges as a result of friction in the boundary layer what leads to reversed flow and changes pressure to suction. The highest values of wind suction on the side walls are close to the edge with the windward wall (in the place of vortices detachment).

Analyzing changes in the angle of wind attack, it can be noted that the lines connecting points of equal pressure values are arranged in parallel to the vertical edges of the model (for angles of wind attack 15°-75°), with a distinct drop near the top due to the 3D flow around the free-end.

Taking into account the surface changes of C_p with respect to different cases of flows, it is observed that for all cases of flow, pressure distributions for all angles are similar. However, there are significant differences in the values of C_p.

Considering the circumferential distributions of C_p it can be observed that the order of plots at a given level is similar for different models. The order changes with levels altitude and along side walls for longer walls. The differences between flows are more apparent in the middle of the wall and exceed 100%. On the other hand, the differences along longer wall as a side wall (the angle equal to 90°) exceed 300% within a single profile and are lower at levels located closer to the base.

Vertical distributions clearly show the influence of the mean wind speed profile on the mean wind pressure coefficient C_p. Above 70 cm (reference point) the sequences of C_p plots and profiles are the same. At lower levels, this relationship is not unique due to the strong influence of the turbulence. Changes of C_p along the height of the model are insignificant in case of profile 1, while for the other profiles, these fluctuations are relatively large.

Connection between C_p and power spectral density functions of the flow is not unique. It can be found that for profile 2 the highest values of the coefficient were obtained at height above 70 cm in each case of the model. The maximum of power spectral density function reaches one of the greatest values at levels above 70 cm for that profile. Similar remarks can be formulated for profile 6, for which the maximum of power spectral density function is even higher, but the pressure coefficient values are slightly lower. The comparison of spectra for profiles 2 and 6 shows that for low frequencies the higher values of the spectrum were obtained for profile 2, which probably results in higher values of pressure although wind speed is greater for profile 6.

CONCLUSIONS

On the basis of presented results and analyses some general remarks can be formulated.

Distribution of pressure coefficient is strongly affected by the wind structure characteristics. The influence of the mean wind speed profile is clear whereas the effect of power spectral density function and turbulence needs to be investigated in details.

The significant differences appear between values of C_p in various cases of approaching flow.

There are also large fluctuations of C_p along the height and circumference within single profile.

Aspect ratio of the models has the influence on values of C_p but the sequences of plots remains the same.

Patterns of C_p for various angles of wind attack are similar for all cases of flows and between models.

Further considerations will be focused on estimation of local and global drag and lift force coefficients to find differences in wind action with respect to wind structure and the angle of wind attack. Such results will give more clear explanation of these dependencies. Moreover, also 3D CFD simulations are under considerations.

REFERENCES

Bęc J., Lipecki T., Błazik-Borowa E. (2011): *Research on wind structure in the wind tunnel of Wind Engineering Laboratory of Cracow University of Technology*, Journal of Physics: Conference Series Vol. 318, 072003, doi: 10.1088/1742-6596/318/7/072003

Cheng C. M., Tsai M. S. (2009): *Along wind design wind load for tall buildings (I) Results of wind tunnel tests*, The 5th International Advanced School on wind Engineering, The GCOE Program at Tokyo Polytechnic University. Opole, Poland

Li Q. S., Melbourne W. H. (1999): *The effects of large-scale turbulence on pressure fluctuations in separated and reattaching flows*, Journal of Wind Engineering and Industrial Aerodynamics, Vol. 83, pp. 159-169

Liang S., Li Q. S., Liu S., Zhang L., Gu M. (2004): *Torsional dynamic wind loads on rectangular tall buildings*, Engineering Structures, Vol. 26, pp. 129–137

Liang S., Liu S., Li Q. S., Zhang L., Gu M. (2002): *Mathematical model of acrosswind dynamic loads on rectangular tall buildings*, Journal of Wind Engineering and Industrial Aerodynamics, Vol. 90, pp. 1757–1770

Lin N., Letchford C., Tamura Y., Liang B., Nakamura O. (2005): *Characteristics of wind forces acting on tall buildings*, Journal of Wind Engineering and Industrial Aerodynamics, Vol. 93, pp. 217–242

Lipecki T., Błazik-Borowa E., Bęc J. (2011): *Wind structure influence on surface pressures of rectangular cylinders at various angles of wind attack*, 13th International Conference on Wind Engineering, July 10-15. Amsterdam, Holland.

Lipecki T., Jamińska P., (2012): *The influence of wind structure and aspect ratio of circular cylinders on mean wind pressure coefficient*, XX Polish Fluid Mechanics Conference, Gliwice, Poland

Miyata T., Miyazaki M. (1979): *Turbulence effects on aerodynamic response of rectangular bluff cylinders*, Proc 5th International Conference on Wind Engineering, 1979, Fort Collins, USA

Nakamura Y., Hirata K. (1989): *Critical geometry of oscillating bluff bodies*, Journal of Fluid Mechanics, Vol. 208, pp. 375-393

Tamura Y., Kikuchi H., Hibi K. (2008): *Peak normal stresses and effects of wind direction on wind load combinations for medium-rise buildings*, Journal of Wind Engineering and Industrial Aerodynamics, Vol. 96, pp. 1043–1057

Wacker J., (1994): *Towards reliability-based local design wind pressures for simple rectangular-shaped buildings*, Journal of Wind Engineering and Industrial Aerodynamics, Vol. 53, pp. 157-175

Zhang J., Gu M. (2009): *Distribution of background equivalent static wind load on high-rise buildings*, Front. Archit. Civ. Eng. China, Vol. 3(3), pp. 241–248